Magnetization reversal processes in magnetic bicrystal junctions

R. Gunnarsson
Department of Microtechnology and Nanoscience (MC2), Chalmers University of Technology, SE-412 96 Göteborg, Sweden

M. Hanson
Department of Applied Physics, Chalmers University of Technology, SE-412 96 Göteborg, Sweden
(Received 12 October 2005; revised manuscript received 8 December 2005; published 31 January 2006)

We provide experimental data for the magnetoresistance in epitaxial ferromagnetic manganite ($La_{0.7}Sr_{0.3}MnO_3$) bicrystals with various angles. Experiments were conducted using samples with in-plane magnetization as well as with out-of-plane magnetization. From the shape of the magnetoresistance hysteresis we draw conclusions on the different magnetization reversal processes. We show that it is possible to set the electrode magnetization at remanence such that the spins at the bicrystal interface are either parallel or inclined to each other at an angle determined by the crystal orientations. Finally, we demonstrate the feasibility of using epitaxial magnetic bicrystals to probe the transport properties in magnetic junctions with well-determined angles of magnetization.

DOI: 10.1103/PhysRevB.73.014435 PACS number(s): 75.70.−i, 75.60.−d, 75.47.−m, 85.75.−d

I. INTRODUCTION

The magnetic tunnel junction (MTJ) has rapidly become one of the most important concepts in the field of "spin electronics."[1] An MTJ consists of two conducting ferromagnets separated by a thin (tunneling) barrier. The most commonly used measure of the performance of a MTJ is its junction magnetoresistance (JMR). In a simple configuration, the spins of the two electrodes are considered to switch between a parallel and an antiparallel alignment. For this case Julliere[2] has given a relation between the JMR magnitude and the polarization of the spins in the electrodes. If the spins are inclined by an angle Θ on the opposing sides of the barrier, it is reasonable to introduce an angular dependence of the conductance and, actually, by theoretically matching the free-electron wave functions in the tunneling barrier Slonczewski[3] arrived at a cosine dependence for the tunneling conductance $G_{sp} \propto \cos\Theta$. The angular dependence has been experimentally corroborated using planar magnetic junctions (two ferromagnetic layers separated by an insulating layer). Moodera and Kinder[4] found a cosinelike dependence on the direction of magnetic field in the resistance of a magnetic tunnel junction $CoFe/Al_2O_3/Co$, and Jaffrés *et al.*[5] demonstrated the conductance of a $Co/Al_2O_3/Co$ junction fitting well to a cosine expression.

Yet another system of magnetic junctions has recently attracted much attention—epitaxial magnetic bicrystals.[6,7] Epitaxial bicrystal junctions comprise devices where a grain boundary (GB) forms a barrier between two ferromagnetic crystals, in which the directions of magnetization can be well defined through monitoring the magnetocrystalline anisotropy. It has been demonstrated that manganite grain boundaries can act as tunnel junctions.[8–13] However, previous studies of the transport in manganite bicrystals have mainly neglected the details of the magnetic configuration of the electrodes and therefore have not included the variation of the inclination between the tunneling spins. The aim of the present study is therefore twofold: (i) to show that it is possible to trace the magnetization reversal from the bicrystal JMR and (ii) to demonstrate the feasibility of using magnetic bicrystal devices to challenge the magnetization direction dependence of conductance.

In this paper we present results for a set of magnetic tunnel junctions formed by different bicrystals of $La_{0.67}Sr_{0.33}MnO_3$. The emphasis of the work is on the JMR hysteresis and its relation to the magnetization-reversal processes involved as the magnetic field is swept back and forth. We present a model for the magnetization reversal that is consistent with our data as well as previously reported data. We show that it is possible to remove the field and leave the electrodes in a well-defined micromagnetic state where the influence of an external magnetic field can be excluded. Thereby we demonstrate the feasibility to use magnetic bicrystals to study the transport properties of MTJ's with electrodes having well-defined directions of magnetization.

The paper is organized as follows: First we present the bicrystal samples of the study. Then we discuss the low-field magnetoresistance and argue that we can obtain the direction of magnetization by analyzing the magnetoresistance data from a micromagnetic energy balance equation. Finally we present new data on the electrical transport of bicrystal MTJ's measured at zero field, thereby demonstrating that magnetic bicrystals can indeed be used to test the angular dependence.

II. SAMPLE DETAILS AND EXPERIMENTAL METHODS

Four bicrystal substrates were selected—three $SrTiO_3$ (STO) substrates, two of which have a symmetric misorientation angle ($\varphi_L = \varphi_R$, L=left, R=right) and one an asymmetric ($\varphi_L \neq \varphi_R$) angle, and one $LaAlO_3$ (LAO) bicrystal substrate with a symmetric misorientation angle. All bicrystals are of (001)-tilt type, meaning that the grains are in-plane misaligned (see Fig. 1), while the (001) planes of the left and right sides are parallel. The angular configuration is defined in Fig. 1, and an overview of the bicrystal samples, with the misorientation angles φ, is given in Table I. Thin films of

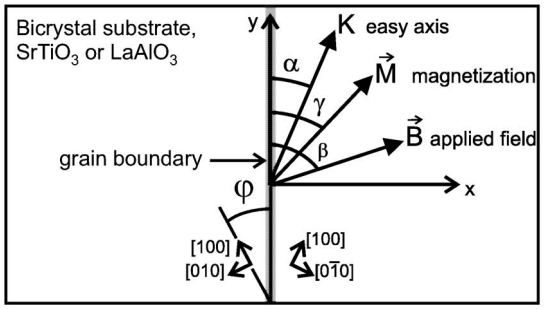

FIG. 1. Drawing of a bicrystal, with definitions of the angles α, β, and γ for the easy axis, the magnetic field, and the magnetization, respectively. The bicrystal misorientation angle φ is the angle between the y axis (the grain boundary) and the [100] directions.

$La_{0.67}Sr_{0.33}MnO_3$ (LSMO) were deposited on the substrates with the conventional pulsed-laser deposition technique. In brief, the deposition parameters were laser wavelength $\lambda = 248$ nm, fluence ~ 1.3 J/cm^2, substrate temperature $T_s = 800$ °C, and growth rate ~ 0.1 Å/pulse. The films were 100 nm thick, estimated from the number of pulses. The surfaces of the films grown on $SrTiO_3$ were flat, as observed by atomic force microscopy. The roughness of the film on $LaAlO_3$ was not estimated, since for other purposes it was covered with a thin gold layer, except for a narrow region around the grain boundary.

X-ray diffractometry (XRD) showed that the films are epitaxial with [001]LSMO and [100]LSMO parallel to [001] and [100], respectively, of the substrate. No indication was found of strain relaxation in the films. The in-plane (a_{in}) and out-of-plane (a_{out}) lattice parameters of the films were found to be $a_{in}^{LSMO/STO} = 3.90$ Å and $a_{out}^{LSMO/STO} = 3.84$ Å on $SrTiO_3$ and $a_{in}^{LSMO/LAO} = 3.79$ Å and $a_{out}^{LSMO/LAO} = 3.95$ Å on $LaAlO_3$. This can be compared to the unstrained bulk value of LSMO, $a_{bulk}^{LSMO} = 3.88$ Å, and the substrates $a^{STO} = 3.90$ Å and $a^{LAO} = 3.79$ Å. Thus, the XRD results show that the in-plane lattice parameter of the films uniquely corresponds to the lattice parameter of the substrate. Hence, LSMO films grown on STO obtain an in-plane tensile strain, whereas those grown on LAO are compressed in plane in relation to the equilibrium (bulk) structure. The total misorientation angle of each film was measured in an x-ray diffraction ϕ scan; see Fig. 2.

TABLE I. Bicrystal sample properties. The misorientation angle, i.e. the direction of [100] with respect to the bicrystal grain boundary (i.e., the y-axis in Fig. 1) is given for the left and right sides as φ_L and φ_R, respectively. The easy direction of magnetization (EA) is given with reference to the crystal directions. Note that the easy direction is in plane for samples A–C and out-of-plane for sample D. The resistance times area product R_0A is obtained for a single junction at 2 K.

Sample	Substrate	φ_L/φ_R	EA	R_0A
A	$SrTiO_3$	12.0°/12.0°	⟨110⟩	160 Ω μm^2
B	$SrTiO_3$	18.4°/18.4°	⟨110⟩	200 Ω μm^2
C	$SrTiO_3$	0/40.0°	⟨110⟩	270 Ω μm^2
D	$LaAlO_3$	9.2°/9.2°	[001]	160 Ω μm^2

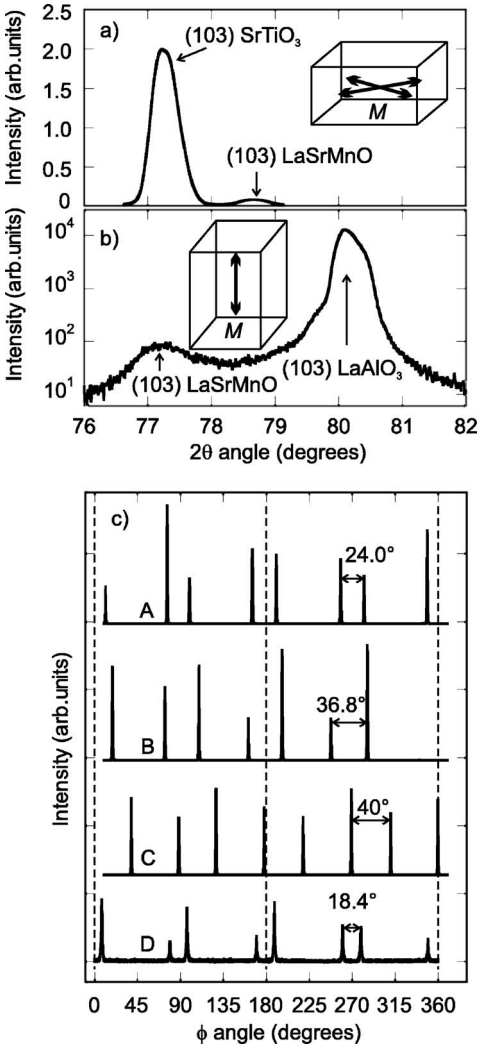

FIG. 2. X-ray diffraction data obtained from the (103) reflections. (a) and (b) $2\theta/\omega$ scans of the LSMO/$SrTiO_3$ and LSMO/$LaAlO_3$ samples, respectively. The wire boxes illustrate the strained unit cells and the directions of the easy axes of magnetization. (c) ϕ scans of the (103)LSMO peaks. The position of the bicrystal grain boundary is indicated by the dashed lines.

A superconducting quantum interference device (SQUID) magnetometer was used for magnetic characterization of the films. Measurements on one LSMO reference sample, grown on a single-crystal STO substrate, demonstrated that at 10 K the easy axes of magnetization are in the ⟨110⟩ in-plane directions, in agreement with previous studies.[14] The magnetic hysteresis—i.e., the magnetization $M(B)$ as function of field B—was measured at 10 K for samples A, B, and C, with the field applied in the in-plane directions parallel to the grain boundary ($B \| \text{GB}$) and perpendicular to it ($B \perp \text{GB}$). Each of the three samples shows almost identical magnetic hysteresis curves when measured in these two directions, as would be expected from the biaxial in-plane symmetry of the films. The coercive field is typically 8 mT for all three samples on $SrTiO_3$. Sample D grown on $LaAlO_3$ was not investigated by magnetization measurements. It is, however, known that whereas the substrate-induced strain from $SrTiO_3$ induces

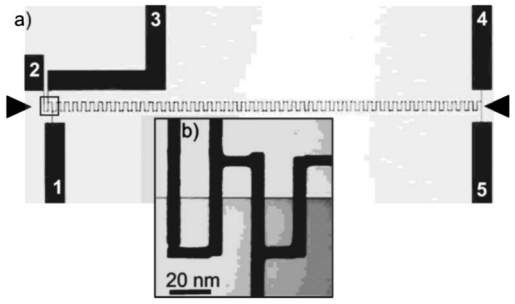

FIG. 3. (a) Micrograph of the meander, with the electrodes numbered. For a single junction the current electrodes are 2 and 4 and the voltage electrodes 3 and 1. The triangles indicate the position of the bicrystal grain boundary. (b) A close-up of the area boxed in (a). The grain boundary is clearly visible.

in-plane magnetocrystalline anisotropy in LSMO, the same film grown on $LaAlO_3$ exhibits an out-of-plane magnetization.[15] Thus, from our structural analysis together with results from other studies[15,16] it is reasonable to conclude that sample D has its easy axis out of plane and that the intermediate magnetization directions along the ⟨110⟩ crystal directions yield an in-plane biaxial anisotropy.

The magnetic tunnel junctions were realized by patterning a meander array of microbridges on each sample using photolithography and Ar-ion milling. The meander contains 100 microbridges, each being about 50 μm long and 6 μm wide; see Fig. 3. The design allows for electrical characterization of a number of grain boundary junctions, from a single junction up to all 105 of them. Gold pads were sputter deposited on top of large contact areas of the LSMO film. Electrical contact to the samples was made by gold-wire bonding in a four-point geometry.

The resistance R of the samples was measured with a bias current of 1 μA, at temperatures ranging from 2 K to 350 K, in a He-flow cryostat with a superconducting solenoid for magnetic fields up to 5 T. The field was applied perpendicular, as well as parallel, to the grain boundary. The curves were measured with the magnetic field swept from a high value, 1 T, thus saturating the samples in one direction, then decreased through zero to the corresponding field in the opposite direction.

For transport measurements, the samples (A–C) were brought to low temperature (2 K) and demagnetized by applying a field of alternating parallel-antiparallel direction and decreasing magnitude. Then the samples were saturated in a magnetic field of 0.5 T, which thereafter was slowly removed at a rate of 0.5 T/min. With $B \perp$ GB the field was set to zero, $B \rightarrow 0$, while for $B \parallel$ GB the field was set to 50 mT. As will be shown in the following this will leave the electrodes in well-defined micromagnetic states. Current-voltage (I-V) characteristics were measured for single junctions at 2 K, and the resistance R was recorded during a slow warm-up ($\sim$1 K/min).

III. MAGNETORESISTANCE

In high fields ($>$0.5 T) the resistance decreases linearly with increasing magnetic field; i.e., dR/dB is constant and

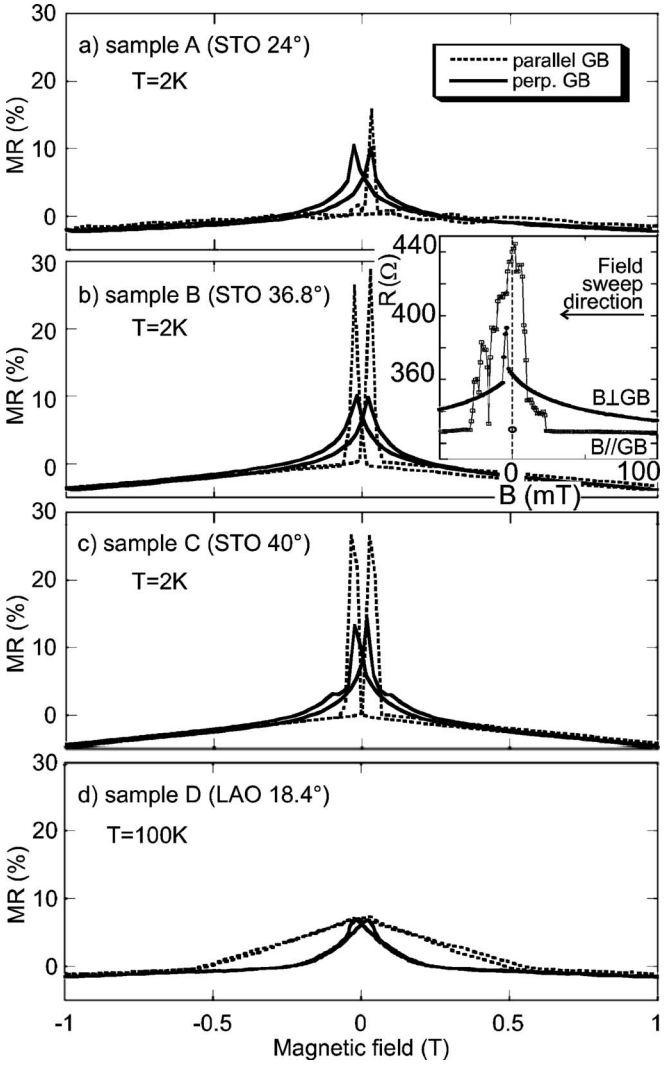

FIG. 4. Magnetoresistance of single junctions measured with the field applied perpendicular (solid line) and parallel (dashed line) to the grain boundary. The magnetic field sweep rate was 0.5 T/min. The inset in (b) shows magnetoresistance data for sample B during a slow field sweep (25 mT/min). The field was swept from saturation. However, to reveal details in the figure only data from 100 mT to −50 mT are shown. The dashed line marks the zero field and the circle marks the resistance R_0 extrapolated from high fields.

negative. An intrinsic resistance at zero field R_0 was obtained by extrapolating the high-field slope to zero field. The value of R_0 at 2 K is 261 Ω, 324 Ω, and 491 Ω for samples A, B, and C respectively. The low-temperature (2 K) resistance times area product (R_0A), shown in Table I, is comparable to what has been reported for other bicrystal junctions (see, e.g., Table 3 in Ref. 17). The overall field dependence of the magnetoresistance $[R(B)-R_0]/R_0$ of a single junction of each sample is shown in Fig. 4 for both field directions. The resistance in low fields is shown in greater detail for sample B in the inset in Fig. 4(b). As can be seen, for both directions of the applied field the resistance peaks around the coercive field, but the shapes of the curves display significant differences. The same kind of behavior is observed for samples A

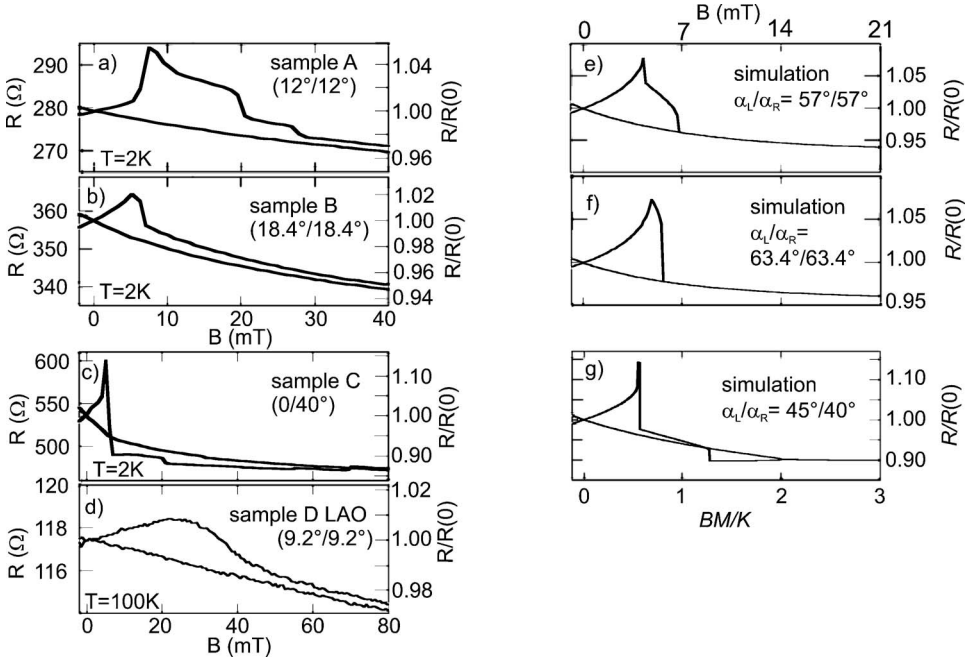

FIG. 5. (a)–(d) Low-field magnetoresistance for samples A–D. The field was aligned perpendicular to the grain boundary and swept with 25 mT/min. (e)–(g) Simulation of the hysteresis using the Stoner-Wohlfarth model for coherent rotation of magnetization. The field is given in units of the reduced magnetic field BM/K The simulations reproduce characteristic details in the magnetoresistance hysteresis of samples A–C. See text for details.

and C. Sample D differs from the others in the case when the magnetic field is applied along the grain boundary. Then the bicrystals with in-plane spontaneous magnetization (samples A–C) exhibit sharp features in a narrow region close to the coercive field, whereas the magnetoresistancce of sample D is broad, triangle like and nonhysteretic. We note that the smearing of the magnetoresistance curve of sample D is not due to the finite temperature (cf. Ref. 18). The characteristics of the parallel and perpendicular field configurations are further discussed below.

A. MR in a field perpendicular to the bicrystal GB

With the field applied perpendicular to the bicrystal interface ($B \perp \mathrm{GB}$) the low-field magnetoresistance varies smoothly. At about 200 mT the resistance starts to increase more rapidly with decreasing field. The resistance has this character of a continuously varying function of the field for all samples, with only a few distinct jumps in some cases. The sharp jumps are especially evident in the resistance of a single junction, but can also be observed in the resistance of a junction array. The shape of the curve and the field where the jumps occur comprise a signature of each sample. This can be clearly seen in Fig. 5. In the next section we will argue that these details can be understood in a picture of coherent rotation of the magnetization through the directions of the easy axes of magnetization (α_L/α_R) for each specific misorientation angle (φ_L/φ_R). The characteristic differences in the magnetoresistance curves are described here. The field where the resistance peaks for samples A, B, and C is 7.0 mT, 5.6 mT, and 5.3 mT, respectively. For sample D this field is 23.5 mT. Further increasing the field above the peak value, sample A has a substantial shoulder extending to 20 mT and, in addition, yet another shoulder extending up to slightly higher fields. Sample B has only an indication of the shoulder feature. The sharpest peak was measured in sample C, where we also observe that the resistance falls to a value *lower* than at the corresponding field when increasing the resistance (decreasing field). There is a tiny shoulder and a fairly long plateau until the resistance just slightly increases and coincides with the resistance measured for a field sweep in the opposite direction. We note that the resistance at zero field, $R(B=0)$, is 279 Ω, 358 Ω, and 537 Ω and the corresponding normalized peak value $R_{peak}/R(B=0)$ is 6%, 2%, and 14% for the samples A, B, and C, respectively. The hysteresis for sample D is smooth, showing a wide hump without any well-defined jumps. The same kind of low-field magnetoresistance hysteresis has been observed in LSMO films grown on single-crystalline, but twinned, $LaAlO_3$.[19]

B. MR in a field parallel to the bicrystal GB

In the $B \| \mathrm{GB}$ case the single-junction resistance remains flat down to about +20 mT, whereafter an irregularly shaped peak appears, with jumps and steps extending down to −30 mT. The position and size of the jumps and steps seem to be randomly varying; however, the effect is always present. When the measurements are performed over several junctions this irregular shape observed for the single junction is absent; the peak in the magnetoresistance hysteresis is smoothed by the averaging over many junctions.

Three previous studies[18,20,21] have been presented, in which the dependence of the magnetoresistance with respect to the direction of applied magnetic field was explicitly studied for single-bicrystal grain boundary junctions. Our observations are consistent with those reports regarding the shape of the hysteresis. However, we did not obtain as sharp hysteresis peaks in the $B \| \mathrm{GB}$ configuration as those observed in the studies by Philipp *et al.*[20] and Todd *et al.*,[21] and in our samples (A–C) the maximum magnetoresistance is typically higher for $B \| \mathrm{GB}$ than for $B \perp \mathrm{GB}$, which also contrasts their reports.

IV. INTERPRETATION OF THE MAGNETIZATION-REVERSAL PROCESS

At high fields, the suppression of spin fluctuations is manifest, known as the colossal magnetoresistance, and the common magnetoresistance that can be observed in Fig. 4 stems from this phenomenon. This effect, which is present in all samples irrespective of the direction of the applied magnetic field, will not be further discussed here. We turn our attention to the low-field magnetoresistance where tunneling effects are observed. Starting from a micromagnetic energy balance equation we will interpret the MR data and draw conclusions about the processes of magnetization reversal and the zero-field remanent states of the electrodes, which evidently differ between the two cases $B \perp$ GB and $B \parallel$ GB.

The magnetic parameters for LSMO can be found in the literature. The magnetic anisotropy energy for LSMO thin films grown on $SrTiO_3$ and $LaAlO_3$ substrates is found to be $K_1^{\mathrm{LSMO/STO}} = -3.9\ \mathrm{kJ/m^3}$ and $K_1^{\mathrm{LSMO/LAO}} = -13\ \mathrm{kJ/m^3}$, respectively.[16] The magnetization for LSMO is $m = 3.6\mu_B$/(Mn site),[22] and the exchange stiffness is $A = 3.0$ meV/Å.[23] The Curie temperature of the samples is $T_c = 350$ K.

A. Magnetization reversal in a field perpendicular to the bicrystal GB and remanent state

The smooth shape of the single-junction MR curves in the $B \perp$ GB configuration suggests that the magnetization reversal occurs by coherent rotation. Indeed, it was recently demonstrated[24,25] that the experimental details in the bicrystal magnetoresistance hysteresis can be recovered using the Stoner-Wohlfarth model for coherent rotation of magnetization. The thermodynamic magnetic free energy $\mathcal{F}$ can be written as a volume integral of the exchange, the Zeeman, the magnetostatic, and the magnetocrystalline anisotropy energy terms[26]:

$$\mathcal{F} = \int \mathrm{d}V(\omega_{ex} + \omega_{Zee} + \omega_{mag} + \omega_{mca}). \tag{1}$$

The exchange energy is determined by the magnetic coupling between nearest neighbors. For a simple cubic lattice the term is $\omega_{ex} = A[(\nabla m_x)^2 + (\nabla m_y)^2 + (\nabla m_z)^2]$, where A is the exchange constant of the material and m_i is the magnetization unit vector projected onto the x, y, or z axis. The Zeeman term in an applied field $\vec{B}$ can be expressed as $\omega_{Zee} = -\vec{M} \cdot \vec{B}$, which in two dimensions becomes

$$\omega_{Zee} = -MB\cos(\gamma - \beta), \tag{2}$$

with γ and β as defined in Fig. 1. Similarly the magnetostatic energy term is $\omega_{mag} = -\vec{M} \cdot \vec{B}_D$, where B_D is the demagnetization field. The magnetostatic energy comes from the self-interaction with the magnetic free poles at the surfaces and can be estimated from $\vec{B}_D = \frac{1}{2} N \cdot \vec{M}$, where $\vec{N}$ is the shape-dependent demagnetization factor.

The magnetocrystalline anisotropy energy is usually described by a phenomenological expression. In the uniaxial case we use $\omega_{mca}^{uni} = K_u \sin^2(\gamma - \alpha)$, where K_u is the first-order uniaxial anisotropy constant and $\gamma - \alpha$ the angle between the magnetization direction and the easy axis; see Fig. 1. For cubic anisotropy the corresponding energy term would be $\omega_{mca}^{cub} = K_1(c_x^2 c_y^2 + c_y^2 c_z^2 + c_z^2 c_x^2)$, with c_i being the directional cosine of the angle $(\gamma - \alpha_i)$ with respect to the i axis. In the biaxial case, where $c_z = 0$, this reduces to

$$\omega_{mca}^{bi} = \frac{K_1}{4} \sin^2 2(\gamma - \alpha). \tag{3}$$

The direction of magnetization γ is obtained by tracing a local energy minimum of Eq. (1) for each specific value of B, starting from the known high-field saturated state. Since the demagnetization factor for the actual sample geometry (100 nm thick, 6 μm wide, and 50 μm long stripes) is small, $N \ll 1$, for in-plane magnetization, the shape anisotropy causes the magnetization to stay mainly in the plane of the film. The magnetization is considered to be homogeneous during coherent rotation, meaning that ω_{ex} is constant. Hence it is sufficient to include only the contributions from Eqs. (2) and (3) to the variations of the magnetic energy. The model presented in Ref. 25 is essentially two dimensional and does not allow for M to be directed out of plane. The magnetic behavior of samples A–C can be analyzed within this model. However, regarding sample D, with its easy axis out of plane, one cannot exclude that other kinds of magnetization processes may take place at the grain boundary.

To account for the electron transport we apply the Slonczewski model[3] for direct tunneling, modified with an additional (constant) non-spin-polarized conductivity contribution. Details of the model can be found in Ref. 25.

Figures 5(e)–5(g) show how the magnetoresistance hysteresis varies with misorientation angle, as obtained from simulations using our model[25] for the present geometry. Each simulation starts from the saturated state in one field direction, and then the direction of magnetization is traced for decreasing fields through zero to saturation in the opposite field direction. The directions of the easy axes are the $\langle 110 \rangle$ in-plane directions. Thus, an additional angle of 45° is added to φ (from Table I) to obtain the direction α of the easy axis. In the simulations we have used $P = 1$ and $G_{ns}/G_s = 7$, where G_{ns}/G_s is the non-spin-polarized current contribution, using the notation in Ref. 25. The result is plotted as a function of the reduced magnetic field BM/K. Using the bulk values for the magnetization and crystalline anisotropy, M and $K_1^{\mathrm{LSMO/STO}}$, as given above, we have $K/M = K_1^{\mathrm{LSMO/STO}}/M \sim 6.8$ mT. As can be seen in Fig. 5 this gives good agreement between the experimental and simulated magnetoresistance curves, although the position of the peak is somewhat shifted towards higher fields in the case of the experiments. This can be explained when considering that the chosen value 6.8 mT actually represents a lower limit of K/M, thus yielding a corresponding lower limit of the peak field. The value of M is obtained using the maximum expected moment $m = 3.6\mu_B$ per Mn site, and the effective anisotropy in a film element is usually higher than the bulk crystalline anisotropy.

We find that the features observed in the low-field response from samples A–C with $B \perp$ GB are well reproduced with the present model; in particular, the prominent features of each sample are recovered. For $\alpha_L/\alpha_R = 57°/57°$ (sample

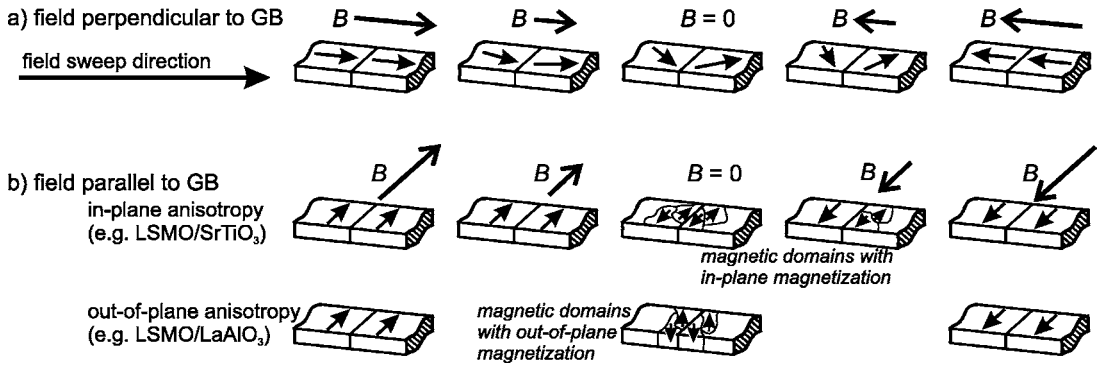

FIG. 6. Suggested directions of magnetization for the electrodes at different stages of the reversal process with the field applied (a) parallel and (b) perpendicular to the bicrystal grain boundary. Magnetic domains are only schematically drawn, and the figure does not necessarily reflect the actual shape of magnetic domains.

A) the simulated magnetoresistance has a substantial shoulder, while for $\alpha_L/\alpha_R=63.4°/63.4°$ (sample B) there is only an indication of the shoulder.[27] The simulated magnitude of the magnetoresistance is about the same in both of the symmetric ($\alpha_L=\alpha_R$) cases. For the asymmetric bicrystal we found that good agreement between the measured hysteresis and the simulation could be obtained for the values $\alpha_L/\alpha_R=45°/40°$. This is somewhat surprising, and the reason is still not clear, since one would expect the easy axis to be parallel to the in-plane $\langle 110\rangle$ directions.[28] However, using $\alpha_L/\alpha_R=45°/40°$, the model can reproduce characteristic features in the experimental resistance curves. The sharp peak, the shoulder, the plateau, and the slight upturn before the resistance coincide with the curve for the opposite direction; all come out nicely from the simulation [see Figs. 5(e)–5(g)].

In the Stoner-Wohlfarth model for coherent rotation, the position of the resistance peak is determined by the reduced magnetic field BM/K. Hence, with a higher anisotropy constant, a higher field is required to reverse the magnetization direction. We note that $K_1^{\mathrm{LSMO/LAO}}/K_1^{\mathrm{LSMO/STO}}\sim 3.3$, which corresponds well to the ratio between the peak fields for sample D and any of the samples A, B, and C. Although the model presented in Ref. 25 is based on the Slonczewski relation[3] for direct tunneling, it should be noted that the choice of transport model does not, all in all, affect the simulated magnetoresistance curve. Specifically the details discussed here are determined solely by the magnetization reversal process. The differences between the experimental data, Figs. 5(a)–5(c), and the simulated magnetoresistance curves, Figs. 5(e)–5(g), in terms of slope ($\mathrm{d}R/\mathrm{d}B$) and magnitude may, however, very well be due to the specific choice of transport model.

Thus, the simulations indicate that the magnetization undergoes a coherent rotation of magnetization when $B\perp\mathrm{GB}$. Then, at remanence after saturation the direction of $\vec{M}$ at $B=0$ is uniquely determined by the direction of the easy axes—i.e., with the system being in a minimum of ω_{mca} as $\gamma-\alpha=0$. With confidence we then consider $R(B=0)$ to be a function of the misorientation angle of the bicrystal, as shown in Fig. 6(b). Thus, from this analysis we deduce the angles between the magnetization directions in the electrodes in the remanent state to be 66°, 53.2°, and 85° for samples A, B, and C, respectively.[29]

B. Magnetization reversal in a field parallel to the bicrystal GB

Then let us discuss the case when the field is applied parallel to the bicrystal interface. Considering the irregular shape of the single-junction peak together with its smoothening when averaged over several junctions, it is obvious that the magnetization reversal involves some stochastic processes in this case. Such a behavior can be expected for domain wall nucleation, movement, and annihilation. To simulate these processes for the current geometry would require an approach with micromagnetic calculations which is beyond the scope of this paper. Here we give a qualitative picture explaining the approach to the zero-field state of the samples. The flat character of the resistance in samples A–C, when brought from high field [inset in Fig. 4(b)], implies that in those samples for fields down to +20 mT the magnetization is not yet broken up into domains, and hence the magnetizations of the two electrodes are parallel. Thus, although there is evidence that the actual remanent state for $B\|\mathrm{GB}$ is split into domains, we can study the state with completely parallel alignment of spins by carefully approaching zero field, $B\rightarrow 0$, down to this low-bias field. Since the anisotropy field $B_{anis}=-K_1/M\simeq 7$ mT is lower than the bias field, we conclude that the magnetization remains aligned along the grain boundary. Then, closer to remanence, domain walls start to nucleate and the magnetic state is split into domains, with possible configurations as schematically illustrated in Fig. 6. The actual value of MR at true $B=0$ is a measure of the total volumes with parallel or antiparallel spin alignment at the grain boundary.

In sample D, due to the out-of-plane anisotropy, the magnetization component perpendicular to the film plane increases with decreasing field. A configuration where some of the domains have their out-of-plane components aligned antiparallel across the grain boundary would lead to a decrease of the magnetostatic contribution to the energy and thus explain the triangular shape of the low-field magnetoresistance of sample D in Fig. 4(d).

At this point we would like to stress that the analysis of the magnetization-reversal process in Secs. IV A and IV B is not restricted to a specific sample or (as in this study) a set of samples. Another manganite bicrystal sample produced by C. Dubourdieu in another laboratory (LMGP-CNRS) has recently been analyzed in a similar way.[30]

V. CHARGE TRANSPORT AT DIFFERENT MICROMAGNETIC STATES

Let us recall the main conclusions from the previous sections: (i) The magnetoresistance of the bicrystal samples under study is consistent with previous reports regarding the shape of the hysteresis. (ii) With $B \| \mathrm{GB}$ the MR hysteresis involves domain wall nucleation, motion, and annihilation. However, when slowly removing the applied field, domain walls do not nucleate until the magnetic field reaches +20 mT (coming from high positive fields); above this field, the magnetization on either side of the tunneling interface remains homogeneous with the magnetization directions of the electrodes staying parallel to each other and directed along the grain boundary. (iii) The case $B \perp \mathrm{GB}$ can be described with a model for coherent rotation of magnetization, without introducing domains down to the true remanent state. The zero-field inclination Θ_0 between the spins in the two electrodes at the bicrystal interface was determined from this analysis.

Then, by the procedure described in Sec. II the magnetization of the electrodes can be set to the well-defined states in which the spins are either parallel ($\uparrow\uparrow$), in the case when an initial field has been applied parallel to the grain boundary, or inclined to each other ($\nwarrow\nearrow$) with the angle Θ_0 when the field has been applied perpendicular to the grain boundary.

Figure 7 shows the temperature dependence of resistance and the *I-V* characteristics for sample C (single junction). There are indeed small differences in the resistance and *I-V* curves for the two configurations ($\uparrow\uparrow$ and $\nwarrow\nearrow$). At low temperature $R_{\uparrow\uparrow}$ is lower than $R_{\nwarrow\nearrow}$ with the difference decreasing with increasing temperature. The *I-V* curves at 2 K are also slightly different depending on the magnetic configuration. Samples A and B behave similar to the shown sample with respect to the temperature and voltage dependence.

We can observe specific features in the voltage dependence of the spin-polarized conductivity. However, the low-voltage noise level (of the order of $10^{-3}\ \Omega^{-1}$) must be reduced in order to make a detailed analysis of the angular dependence. We are presently working on improving the accuracy of the measurement system, and the influence of angle of magnetization on the spin-polarized current will be examined in an extension to the present study.

VI. DISCUSSION

Our analysis of the magnetoresistance of the bicrystals clearly demonstrates its dependence on the angle between the magnetization directions in the electrodes. Furthermore, it gives a means to control the micromagnetic behavior at the bicrystal interface. We are now looking for a proper description of the spin transfer across the interface—including the angle Θ between the spins on either side of the barrier. As discussed in the Introduction, this was previously studied in a planar junction geometry. However, contrary to the planar systems, magnetic bicrystals can be measured at remanence for different angles, without the influence of any external magnetic field.

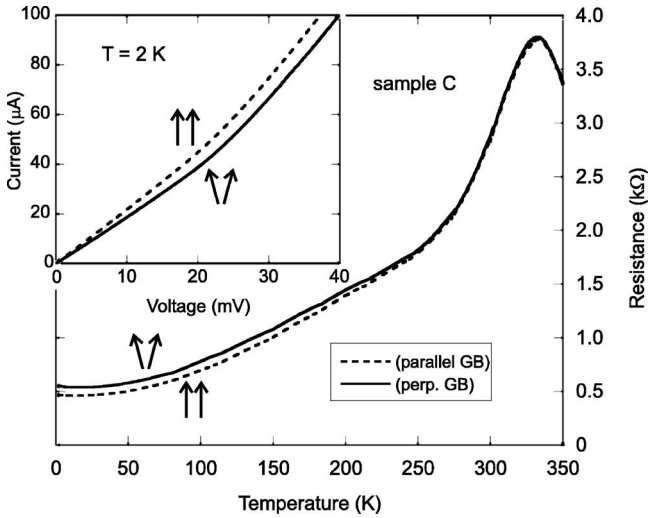

FIG. 7. Resistance at different micromagnetic states ($\uparrow\uparrow$ and $\nwarrow\nearrow$) when the field was removed perpendicular to or parallel to the grain boundary, as indicated in the figure. Data are taken for a single junction of sample C.

On the other hand, the charge transport mechanism across the grain boundary interface in bicrystals is still under discussion. In this study we used Slonczewski's model[3] for direct tunneling between magnetically misaligned electrodes, and indeed tunneling is often mentioned as a possible mechanism. There are also other interpretations of the experimental data, of which hopping in a magnetically disordered region is one of the most applied. Strong support for the presence of a magnetically disordered, or possibly antiferromagnetically ordered, region at the grain boundary comes from magnetoresistance measurements in very high fields,[31] up to 50 T. Doping of the grain boundary region was also shown to influence the conductance.[32] For manganite bicrystals, such as those in the present study, the extension and character of any disordered region should have a bearing on the choice of model. Thus, information about the microstructure of the bicrystals would be of great value. In fact, the grain boundary structure can be very well ordered at the interface[33] and the disordered region can be as narrow as 1 nm, narrow enough for tunneling to occur.

We would like to stress that the actual choice of transport model does not influence the main results in this paper. The details in the magnetoresistance hysteresis are determined by the coherent rotation of the magnetization and the nucleation and motion of magnetic domains. If the conductivity were chosen to have a different angular dependence than directly proportional to the cosine function, the steepness ($\mathrm{d}R/\mathrm{d}B$) of the curves would change, but the characteristic jumps and other features in the resistance curves would still be present at the same fields.

In conclusion, based on the result of this study we are able to control the orientation of the magnetization in magnetic bicrystal junctions and thereby single out the transport properties. As a consequence of this, the results show that magnetic bicrystal systems can be suitable candidates for studying the angular dependence of the low-field magnetoresistance of manganites.

VII. SUMMARY

We have studied bicrystal grain boundary junctions of the ferromagnetic $La_{0.7}Sr_{0.3}MnO_3$ with different misorientation angles. The samples were patterned into microbridges crossing the grain boundary. At high fields (>0.5 T) and low temperatures the behavior is independent of the field direction. However, the magnetoresistance at low field (<0.5 T) is different depending on the direction of the easy axis of magnetization. We can point out features in the magnetoresistance hysteresis that are characteristic for each specific combination of substrate strain and misorientation angle. By micromagnetic arguments we have shown that it is possible to tailor the zero-field (or a low-bias-field) spin configuration at the bicrystal interface; with in-plane anisotropy, the spins of the two electrodes can be aligned in parallel after removal of a field applied parallel to the grain boundary, whereas the spins can be left with a well-defined inclination to each other if a perpendicular field is removed. We used these two configurations to study the voltage and temperature dependence of the conductance. Thereby we have demonstrated the feasibility of using manganite bicrystal junctions to probe the angular dependence of magnetization in magnetic junctions.

ACKNOWLEDGMENTS

R.G. is grateful for the valuable comments by T. Claeson and E. Olsson. We also gratefully thank A. Hahlin for experimental assistance during the SQUID magnetometry. This work has been financially supported by Vetenskapsrådet (VR) and Stiftelsen för Strategisk Forskning (SSF) within the "OXIDE" program.

[1] See, e.g., S. A. Wolf, D. D. Awschalom, R. A. Buhrman, J. M. Daughton, S. von Molnár, M. L. Roukes, A. Y. Chtchelkanova, and D. M. Treger, Science **294**, 1488 (2001); J. F. Gregg, I. Petej, E. Jouguelet, and C. Dennis, J. Phys. D **35**, R121 (2002).
[2] M. Julliere, Phys. Lett. **54A**, 225 (1975).
[3] J. C. Slonczewski, Phys. Rev. B **39**, 6995 (1989).
[4] J. S. Moodera and L. R. Kinder, J. Appl. Phys. **79**, 4724 (1996).
[5] H. Jaffrés, D. Lacour, F. Nguyen Van Dau, J. Briatico, F. Petroff, and A. Vaurés, Phys. Rev. B **64**, 064427 (2001).
[6] N. D. Mathur, G. Burnell, S. P. Isaac, T. J. Jackson, B.-S. Teo, J. L. MacManus Driscoll, L. F. Cohen, J. E. Evetts, and M. G. Blamire, Nature (London) **387**, 266 (1997).
[7] K. Steenbeck, T. Eick, K. Kirsch, K. O'Donnell, and E. Steinbeiss, Appl. Phys. Lett. **71**, 968 (1997).
[8] K. Steenbeck, T. Eick, K. Kirsch, H.-G. Schmidt, and E. Stenbeiß, Appl. Phys. Lett. **73**, 2506 (1998).
[9] J. Klein, C. Höfener, S. Uhlenbruck, L. Alff, B. Büchner, and R. Gross, Europhys. Lett. **47**, 371 (1999).
[10] N. K. Todd, N. D. Mathur, S. P. Isaac, J. E. Evetts, and M. G. Blamire, J. Appl. Phys. **85**, 7263 (1999).
[11] M. Ziese, Phys. Rev. B **60**, R738 (1999).
[12] C. Höfener, J. B. Philipp, J. Klein, L. Alff, A. Marx, B. Büchner, and R. Gross, Europhys. Lett. **50**, 681 (2000).
[13] M. Paranjape, J. Mitra, A. K. Raychaudhuri, N. K. Todd, N. D. Mathur, and M. G. Blamire, Phys. Rev. B **68**, 144409 (2003).
[14] P. Lecoeur, P. Trouilloud, G. Xiao, A. Gupta, G. Q. Gong, and X. W. Li, J. Appl. Phys. **82**, 3934 (1997).
[15] C. Kwon, M. C. Robson, K.-C. Kim, J. Y. Gu, S. E. Lofland, S. M. Bhagat, Z. Trajanovic, M. Rajeswari, T. Venkatesan, A. R. Kratz, R. D. Gomez, and R. Ramesh, J. Magn. Magn. Mater. **172**, 229 (1997).
[16] K. Steenbeck and R. Hiergeist, Appl. Phys. Lett. **75**, 1778 (1999).
[17] M. Ziese, Rep. Prog. Phys. **65**, 143 (2002).
[18] R. Gunnarsson, Z. G. Ivanov, C. Dubourdieu, and H. Roussel, Phys. Rev. B **69**, 054413 (2004).
[19] R. Gunnarsson (unpublished).
[20] J. B. Philipp, C. Höfener, S. Thienhaus, J. Klein, L. Alff, and R. Gross, Phys. Rev. B **62**, R9248 (2000).
[21] N. K. Todd, N. D. Mathur, and M. G. Blamire, J. Appl. Phys. **89**, 6970 (2001).
[22] M. C. Martin, G. Shirane, Y. Endoh, K. Hirota, Y. Moritomo, and Y. Tokura, Phys. Rev. B **53**, 14285 (1996).
[23] We calculate the exchange stiffness as $A=(DS/2)\rho_{\mathrm{Mn}}$ [Weissmüller *et al.*, J. Res. Natl. Inst. Stand. Technol. **104**, 261 (1999)] using the experimental value for the spin-wave stiffness $D=188$ meV Å^2 (Ref. 22).
[24] D. J. García and B. Alascio, Physica B **320**, 7 (2002).
[25] R. Gunnarsson, M. Hanson, and C. Dubourdieu, J. Appl. Phys. **96**, 482 (2004).
[26] A. Aharoni, *Introduction to the Theory of Ferromagnetism* (Oxford University Press, Oxford, 2000).
[27] A more detailed discussion of the angular dependence of the Stoner-Wohlfarth model can be found in R. Gunnarsson and M. Hanson, J. Phys.: Condens. Matter **16**, 3761 (2004).
[28] We did not find good agreement between the experimental data and simulated magnetoresistance using the expected angles $\alpha_L/\alpha_R=45°/95°$.
[29] Due to the biaxial geometry, $\Theta_0=2\beta-\alpha_L-\alpha_R$, except when $\alpha<45°$ (as for sample C), where $\Theta_0=\alpha_L+\alpha_R$.
[30] R. Gunnarsson, M. Hanson, and C. Dubourdieu, J. Magn. Magn. Mater. **290-291**, 761 (2005).
[31] N. Kozlova, K. Dörr, D. Eckert, T. Walter, and K.-H. Müller, J. Magn. Magn. Mater. **261**, 48 (2003).
[32] M. G. Blamire, C. W. Schneider, G. Hammerl, and J. Mannhart, Appl. Phys. Lett. **82**, 2670 (2003).
[33] T. Liljenfors, R. Gunnarsson, and E. Olsson (unpublished).